JOURNAL OF MATERIALS SCIENCE **34** (1999) 4311–4320

Structure and properties of rapidly solidified Mg-Al alloys

S. S. CHO, B. S. CHUN, C. W. WON, S. D. KIM, B. S. LEE, H. BAEK
Rapidly Solidified Materials Research Center (RASOM), School of Materials Engineering, Chungnam National University, Taedok Science Town, Taejon 305-764, South Korea

C. SURYANARAYANA
Department of Metallurgical and Materials Engineering, Colorado School of Mines, Golden, CO 80401-1887, USA
E-mail: schallap@mines.edu

Three binary Mg-Al alloys containing nominally 5, 15, and 30 at % Al were prepared in the ingot and rapidly solidified flake conditions using the twin roll technique. The microstructure, mechanical properties, and electrochemical behavior of the extruded alloys in both the conditions were investigated. The hardness, tensile strength, and corrosion resistance increased with increasing Al content. Further, the hardness, tensile strength, and corrosion resistance of the rapidly solidified alloys were superior to the ingot-metallurgy alloys and this is attributed to the microstructural refinement and increased homogeneity in the rapidly solidified alloys.

1. Introduction

The ever-increasing demands for lightweight alloys in the aerospace and automobile industries have led to the development of novel materials and advanced processing techniques which exploit processing of materials at far-from-equilibrium (or non-equilibrium) conditions [1]. Rapid solidification from the liquid state is an important non-equilibrium processing technique and has been frequently employed to improve the properties and performance of existing alloys and also for the development of entirely new compositions. A recent review summarizes the developments on these aspects of lightweight alloys [2].

Rapid solidification involves cooling of metallic melts at rates $>10^4$ K/s and results in significant microstructural and constitutional changes. The microstructural modifications include grain refinement and reduced segregation effects while the constitutional changes include formation of supersaturated solid solutions, and metastable crystalline intermediate and amorphous phases [3, 4]. These effects, either alone or in combination, have improved the mechanical behavior and performance of the rapidly solidified alloys (in comparison to the ingot metallurgy (IM) alloys) and these results were especially significant for lightweight metals and have been well documented in the literature [1–5].

Even though rapid solidification processing (RSP) has been extensively applied to amorphous alloys [4, 6–9], several aluminum [2, 4, 5] and titanium [4, 5, 10] alloys, it has been used only to a limited extent for magnesium-base alloys [5, 11–14]. Magnesium is a very light metal (density is 1.74 g/cm^3) and thus can find useful applications in the aerospace and automobile industries. Magnesium alloys, however, have a low tensile strength and poor corrosion resistance and thus their applications are limited. Hence, there exists an urgent need to improve the strength and corrosion resistance of magnesium alloys.

Additions of aluminum to magnesium increase the strength and corrosion resistance of Mg-Al alloys [15]. Since RSP results in increased solid solubility limits and refinement of microstructural features, RSP alloys usually exhibit strengths higher than those of IM alloys. Further, because of the homogeneity of microstructure, RSP alloys are also expected to exhibit better corrosion resistance than their IM counterparts [16–21]. Thus, the aim of the present investigation is to evaluate the microstructure, mechanical properties, and corrosion behavior of rapidly solidified binary Mg-Al alloys containing nominally 5, 15, and 30 at % Al and compare them with their IM counterparts.

Under equilibrium conditions, aluminum has a limited solid solubility in Mg; it is only <1 at % at room temperature. The solid solubility increases with temperature and reaches a value of 11.8 at % at the eutectic temperature of 437 °C [22]. Thus, under equilibrium conditions, all the alloys used in the present investigation consist of the Mg(Al) solid solution (from now on referred to as α-Mg) and the Mg-rich intermetallic phase β-$Mg_{17}Al_{12}$.

2. Experimental

Binary Mg-Al alloys containing nominally 5, 15, and 30 at % Al were prepared by melting the pure metals Mg and Al in the desired proportions. The chemical analysis of these alloys in the as-cast condition is presented in

TABLE I Chemical analysis of the binary Mg-Al alloy ingots and flakes

Condition	Nominal Al content (at %)	Analyzed Al content (at %)
Ingot	5	5.2
	15	16.2
	30	31.7
Flake	5	5.7
	15	14.7
	30	33.1

Table I. From now onwards when we refer to an alloy composition, it will be the nominal composition of the alloy in atomic percent.

Ingots of these three compositions were hot extruded (in the temperature range of 290–350 °C) with an extrusion ratio of 24 : 1 and at an extrusion velocity of 33 mm/sec.

Thin flakes (100–300 μm in thickness) of these three alloys were produced by the twin-roll technique of RSP under the following experimental conditions:

Roll diameter	368 mm
Nozzle diameter	5.0 mm
Roll velocity	800 rpm
Pouring rate	2.1 kg/min

Chemical analysis of the RSP flakes (Table I) confirmed that the aluminum content in the rapidly solidified alloys is close to the starting nominal value.

The flakes produced were then cold compacted to 80% of the theoretical density, degassed at 350 °C for 1 h under a vacuum of 10^{-2} torr and then hot extruded under conditions similar to those of the ingot. Thus, the three different alloy compositions were investigated in four different conditions:

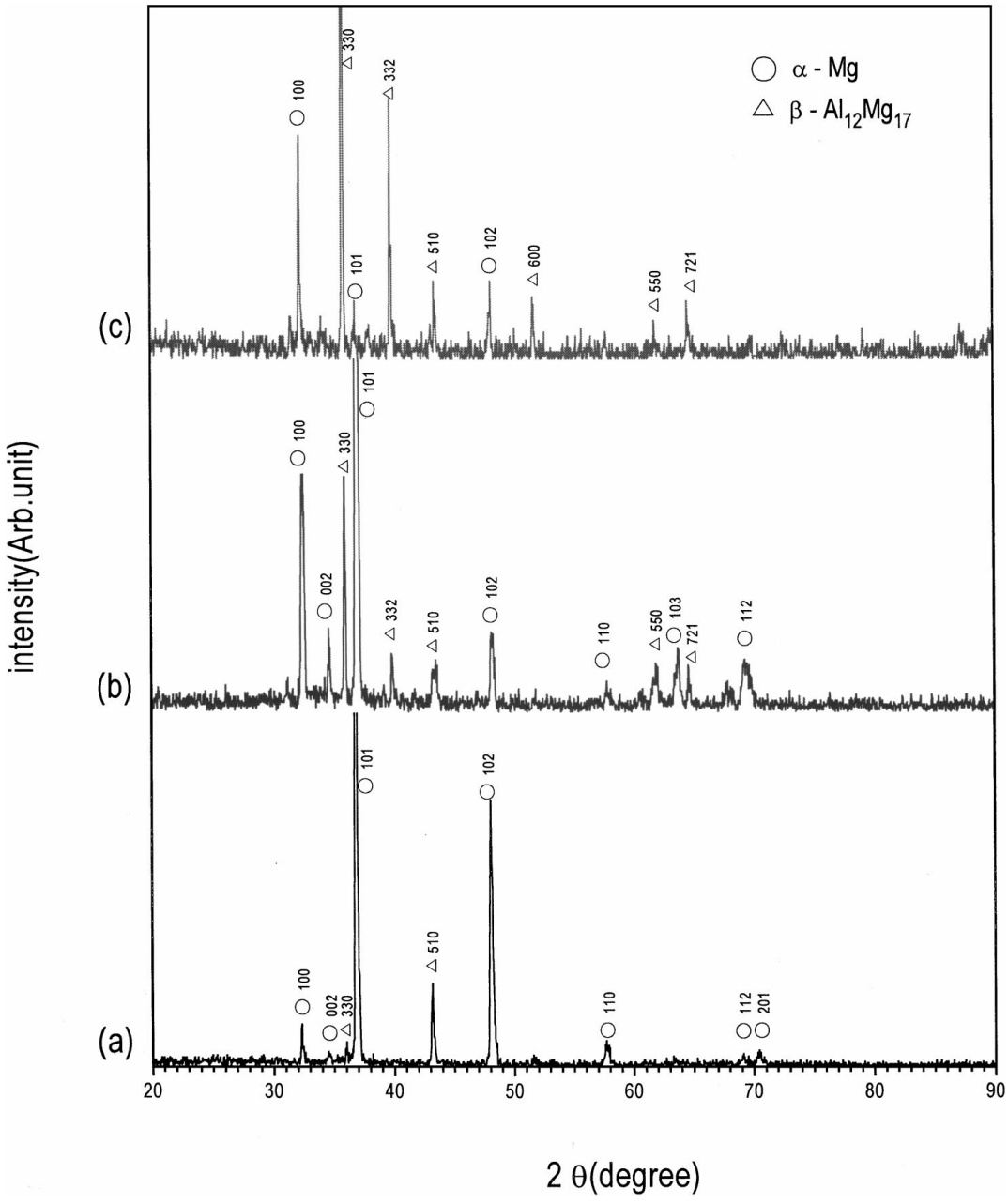

Figure 1 X-ray diffraction patterns of the Mg-Al ingots. (a) Mg-5Al, (b) Mg-15Al, and (c) Mg-30 Al.

(i) ingot as-cast condition
(ii) ingot as-extruded condition
(iii) flake as-solidified condition
(iv) flake as-extruded condition

Materials in these four conditions were examined by optical and scanning electron microscopy (SEM) techniques for their microstructural features, and by X-ray diffraction (XRD) technique for the crystal structure features. Scanning electron microscopy was done on an ISI-DS130 SEM and XRD was conducted on a Siemens JSDM510 diffractometer using CuK_α radiation. The hardness of the materials was measured using a Vickers hardness tester with a load of 1 kg and the tensile strength and elongation were evaluated using an MTS machine. The fracture surfaces were examined in the SEM. Electrochemical tests were conducted using an EG&G 273A potentiostat.

3. Results and discussion

3.1. Phase constitution

Fig. 1 shows the X-ray diffraction patterns of the Mg-5, 15, and 30 Al ingots. All the diffraction patterns contain peaks due to both the α-Mg and β-$Mg_{17}Al_{12}$ phases. The peak positions for the α-Mg phase are consistent with a hexagonal close-packed structure with the lattice parameters $a = 0.3203$ nm, $c = 0.5203$ nm, and $c/a = 1.624$, and those for the β-$Mg_{17}Al_{12}$ phase with a cubic structure with $a = 1.063$ nm. It may also be noted that the amount of the β-$Mg_{17}Al_{12}$ phase increased with increasing Al content in the alloys.

Fig. 2 shows the X-ray diffraction patterns of the alloy flakes of the three compositions. The same α-Mg and β-$Mg_{17}Al_{12}$ phases present in the ingot are also present in the RSP flakes. However, because of the rapid solidification effects, a significant amount of Al has dissolved in Mg forming supersaturated solid solutions in

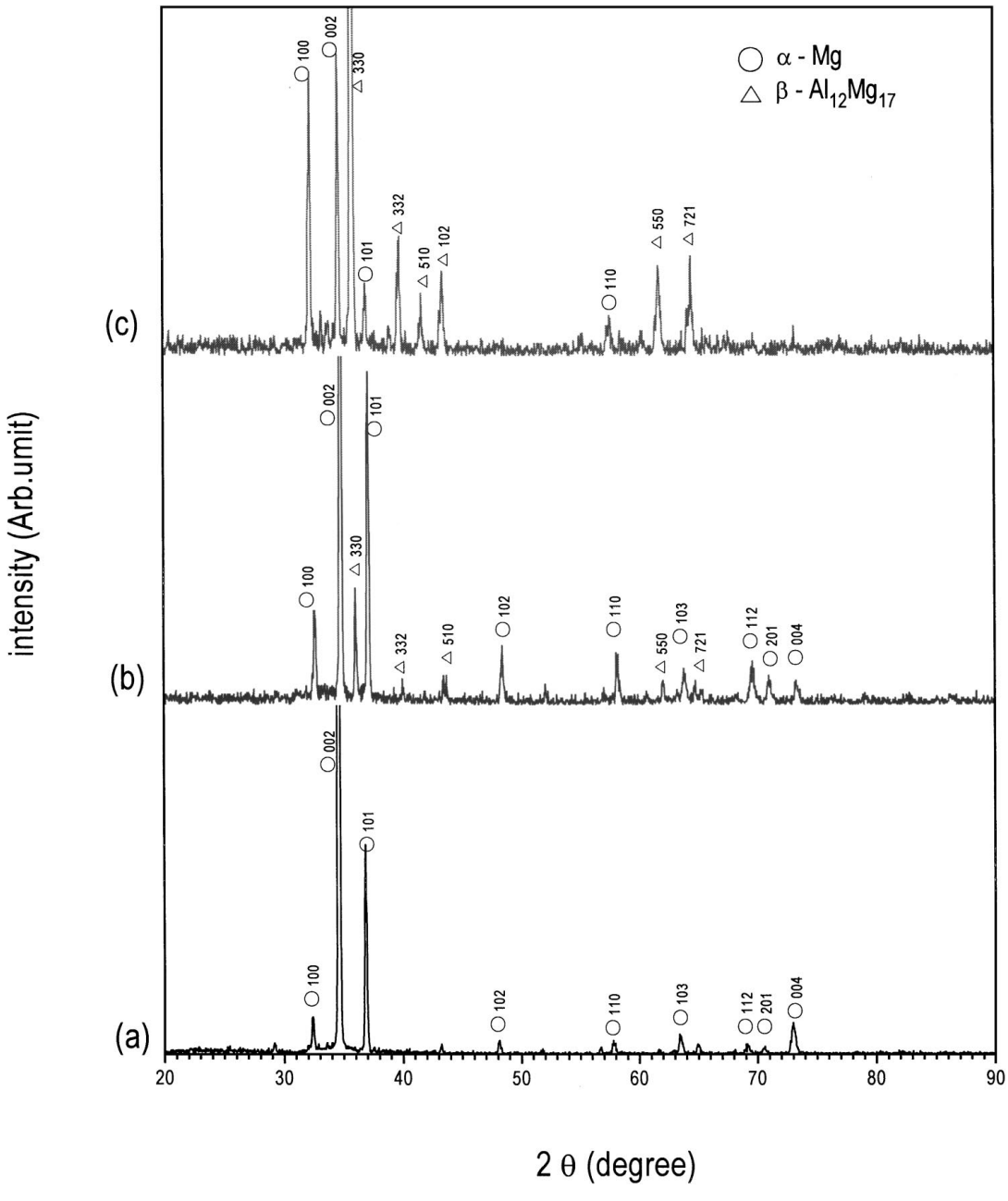

Figure 2 X-ray diffraction patterns of the rapidly solidified Mg-Al flakes. (a) Mg-5Al, (b) Mg-15Al, and (c) Mg-30Al.

all the compositions. Accordingly, the Mg-5Al alloy flake shows the presence of only the α-Mg phase, suggesting that all the Al has gone into Mg to form the supersaturated solid solution. In other compositions also, supersaturated solid solutions have formed. This is inferred from the shift of the α-Mg peaks to higher angular positions and consequently the α-Mg solid solution phase had smaller lattice parameters than pure Mg (Fig. 2). Measurement of the peak positions of the α-Mg phase clearly indicates that the maximum decrease in lattice parameters is obtained in the Mg-15Al alloy and that the lattice parameters of the α-Mg phase in this alloy composition are $a = 0.3168$ nm, $c = 0.5156$ nm, and $c/a = 1.627$. From a knowledge of the variation of lattice parameters with Al content [23], the maximum solid solubility of Al in Mg in the present rapidly solidified alloys was estimated to be 10.6 at % Al. This value is qualitatively in agreement with the observation that while only the α-Mg phase is present in the RSP Mg-5Al alloy, both α-Mg and β-$Mg_{17}Al_{12}$ phases are present in the RSP Mg-15 and 30 Al alloys. Because of the increased solid solubility of Al in Mg in the RSP alloys, the relative proportions of the α-Mg and β-$Mg_{17}Al_{12}$ phases are different in the Mg-15 and 30 Al alloys in the flakes and the ingots. Much higher solid solubility levels have been reported in RSP Mg-Al alloys reaching values as high as 22.6 at % Al in Mg [23]. But, this high supersaturation was obtained by rapidly solidifying the alloys using the "gun" technique which is known to produce much higher solidification rates than the twin roll technique used in the present investigation [24].

Another important point emerges from a comparison of Figs 1 and 2. The $(1\,0\,1)_{Mg}$ reflection has a much higher intensity than the $(0\,0\,2)_{Mg}$ reflection in the ingot material. On the other hand, the $(0\,0\,2)_{Mg}$ reflection has the highest intensity in the rapidly solidified flake material. This is an indication of the occurrence of preferred orientation in the flake material because of the spread of the melt on the conducting substrate. Preferred orientations in RSP materials have been reported earlier [25, 26].

3.2. Microstructure

Fig. 3 shows optical micrographs of the three Mg-Al alloy ingots. One can see that the microstructure consists of two constituents—the α-Mg solid solution and the eutectic. The eutectic constituent present along the grain boundaries increases in amount with increasing Al content and the microstructure in the Mg-30Al alloy is almost completely made up of the eutectic constituent. This is expected from the fact that a eutectic reaction occurs near this composition in the Mg-Al system.

Fig. 4 shows the optical micrographs of the rapidly solidified flakes in both the transverse and longitudinal directions. Well-defined dendritic structures are seen in the transverse direction and it may also be noted that the dendrite arm spacing is fine. For example, it is about 2 μm in the RSP Mg-15Al flakes. Such fine dendrite arm spacings can be related to the high solidification rates experienced during RSP. Kattamis *et al.* [27] related the dendrite arm spacing, d (in μm) of Mg-5wt% Zn alloys to the local solidification time, t (in seconds) and established the relationship $d = 10.5 \times t^{0.4}$. Since the thermal conductivity of the alloys decides the solidification times, this same relationship is not going to be exactly valid for the Mg-Al alloy system; but, the differences may not be very significant. Using this relationship and also those established for other alloy systems [25], it was estimated that the Mg-15Al alloy solidified at approximately 1.3×10^4 K/s. One cannot discern many microstructural details in the micrographs (Fig. 4) at these low magnifications, except to mention that the microstructural features are finer in the RSP alloys than they are in the IM alloys.

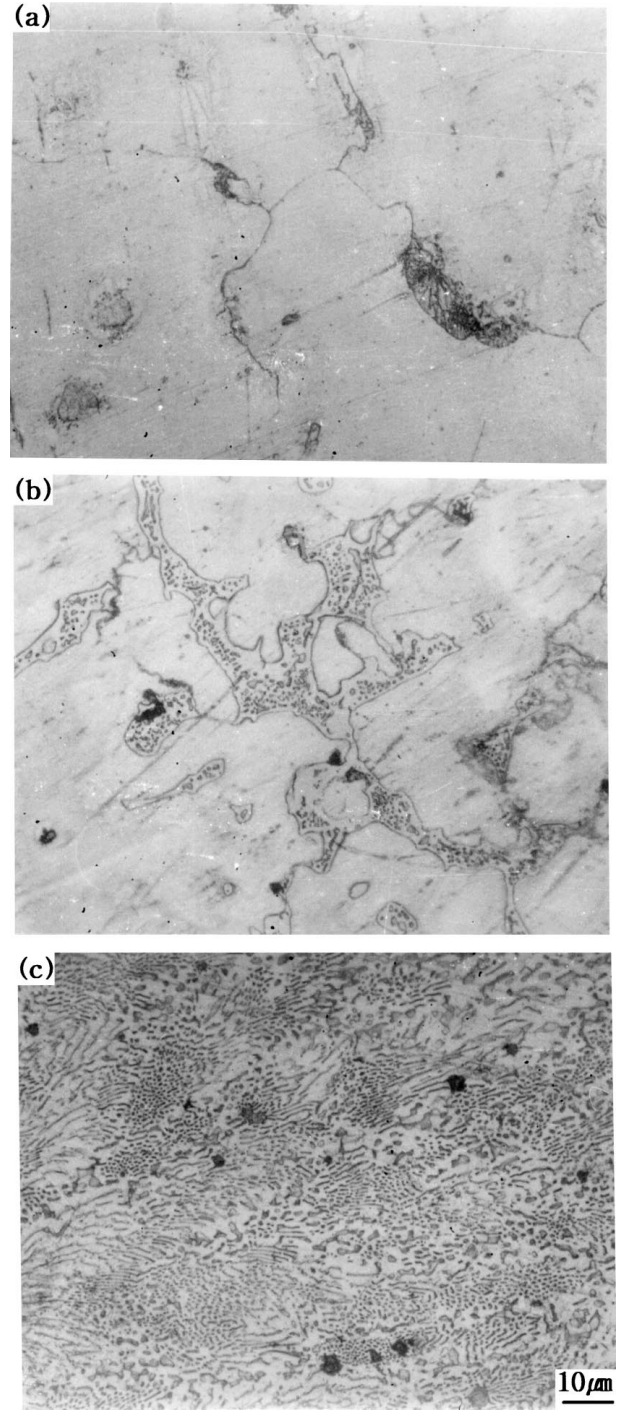

Figure 3 Optical micrographs of as-cast Mg-Al ingots. (a) Mg-5Al, (b) Mg-15Al, and (c) Mg-30Al.

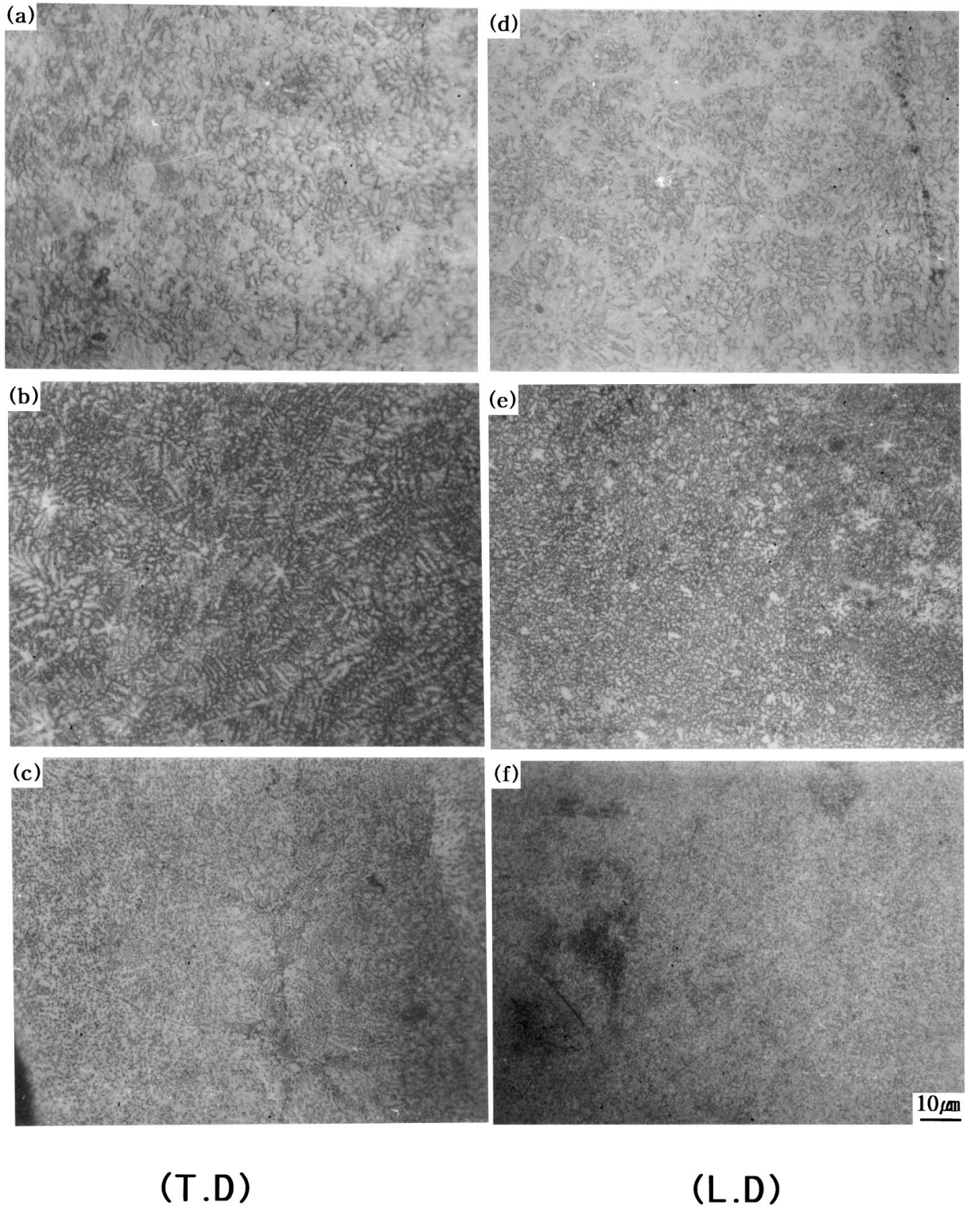

Figure 4 Optical micrographs of the RSP flakes in the (a)–(c) transverse and (d)–(f) longitudinal sections. (a) and (d) Mg-5Al, (b) and (e) Mg-15Al, and (c) and (f) Mg-30Al.

Fig. 5a and b show optical micrographs of the extruded Mg-5Al alloy ingot and flakes, respectively. Both the microstructures show equiaxed grains, mostly due to the recrystallization that has occurred during extrusion. It should be, however, noted that while the grain size of the extruded ingot is about 30 μm, that of the extruded flake material is only about 10 μm. This is related to the original grain size of the ingot and flake, respectively; the former had a coarser grain size.

Another feature worth noticing in the above micrographs is that in both the cases, there appears to be some fine structure inside the grains. Fine equiaxed structures and increased amounts of precipitation are observed in alloys with higher Al contents. The fine structure could be due to either (a) precipitation of a second phase, or (b) formation of etch pits because of deep etching. The first option may not be true at least in the ingot material. This is because, according to the phase diagram, the solid solubility of Al in Mg is higher at higher temperatures (of extrusion, for example) than it is at room temperature and therefore more Al would have gone into solid solution. Consequently,

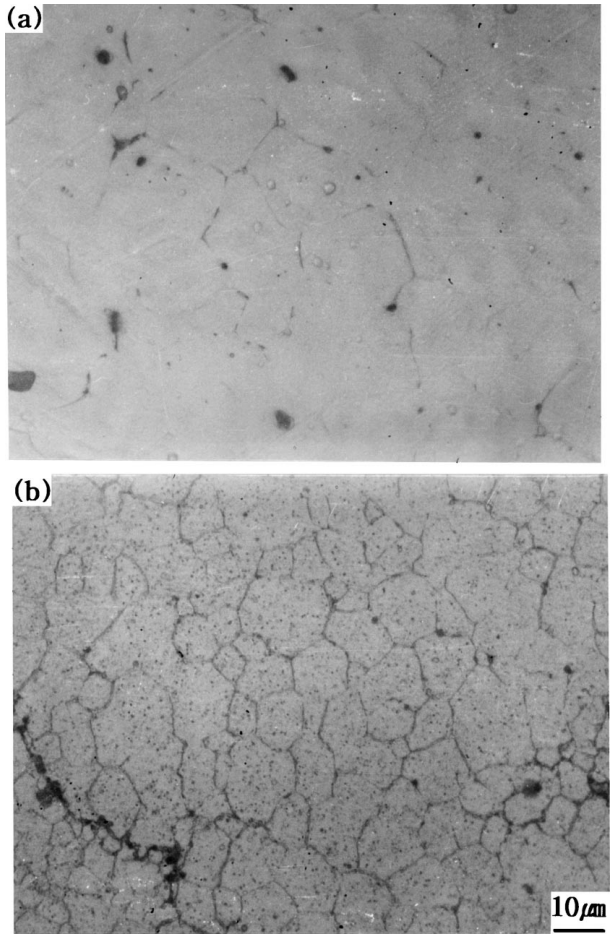

Figure 5 Optical micrographs of the Mg-5Al extrusions (a) ingot, (b) flake.

precipitation of a second phase would not occur. In the flake extrusion, however, it is possible that because of the supersaturation achieved during RSP, the excess Al has precipitated out during the hot extrusion process. This can be confirmed only with the help of other techniques such as X-ray diffraction (if the amount of precipitate is large enough) and/or transmission electron microscopy. X-ray diffraction patterns of the Mg-5Al flake extrusion confirm the presence of the β-$Mg_{17}Al_{12}$ phase (Fig. 6) and thus it is possible that the internal structure in Fig. 5b is due to precipitation of the β-$Mg_{17}Al_{12}$ phase. Note that the preferred orientation in the flakes has disappeared after extrusion, probably due to the recrystallization at the relatively higher temperature of extrusion. Consequently, the intensities of the different reflections in the X-ray diffraction pattern are as expected from the standard equiaxed material. In the ingot extrusion, however, the small amount of internal structure may be due to the etching effects.

3.3. Mechanical properties

The hardness of the three alloys in the as-cast ingot and flake conditions is presented in Fig. 7. The hardness of the alloys increased with increasing Al content; it increased from about 50 VHN for the Mg-5Al ingot to about 185 VHN for the Mg-30Al ingot. The flake material has a higher hardness than the ingot material, essentially due to the fine microstructure. The hardness value of the flakes also increased from about 60 VHN

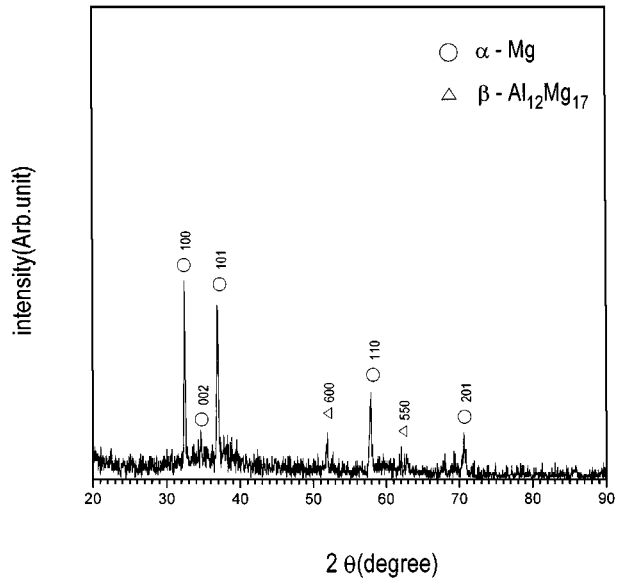

Figure 6 X-ray diffraction pattern of the Mg-5Al flake extrusion.

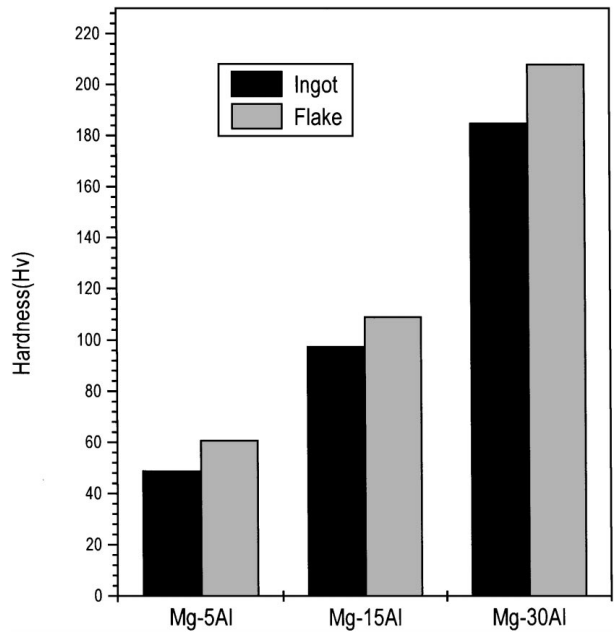

Figure 7 Hardness values of the Mg-5, 15, and 30Al ingots and flakes.

for Mg-5Al to about 210 VHN for Mg-30Al. The as-extruded ingot and flake products also have almost the same hardness values as the as-cast ingot and flake products, respectively. Thus it appears that the hardness is not significantly different in the as-cast and extruded conditions. This is a little surprising since some recrystallization took place during the hot extrusion process.

The tensile properties of the extrusions from the ingot and flakes are shown in Fig. 8 for the Mg-5Al and Mg-15Al compositions. It may be again noted that the tensile strength increases with increasing Al content and consequently the elongation decreases. Further, mirroring the behavior of hardness values, there does not appear to be any meaningful difference in the tensile properties of the ingot and flake materials in the as-cast and extruded conditions.

A point of interest in this connection is that while the magnitude of increase in hardness from the Mg-5Al to Mg-15Al is about 80%, that in tensile strength is only

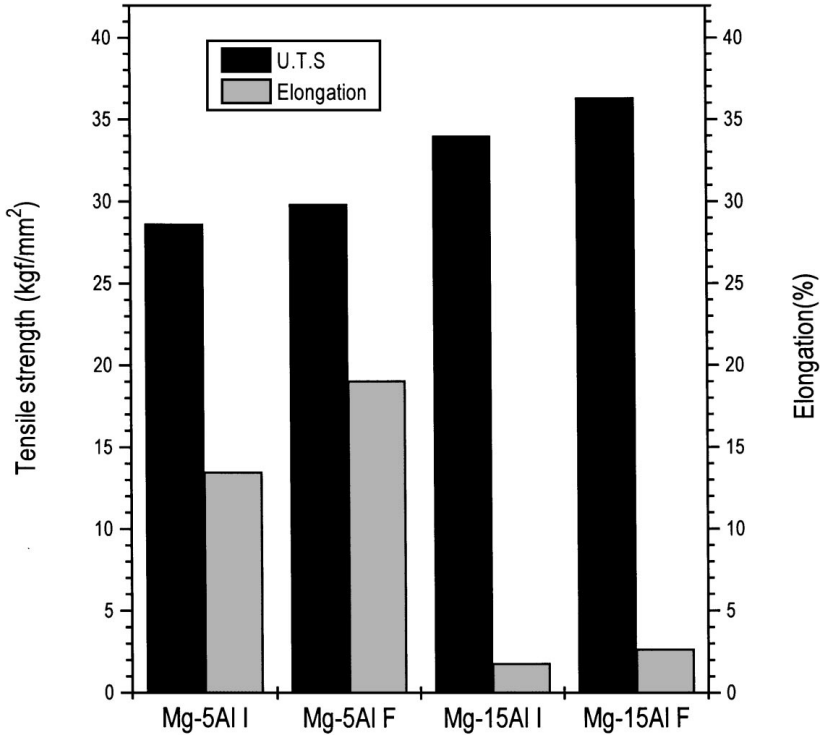

Figure 8 Tensile strength and elongation of extrusions from the ingots and flakes of Mg-5Al and Mg-15Al alloys.

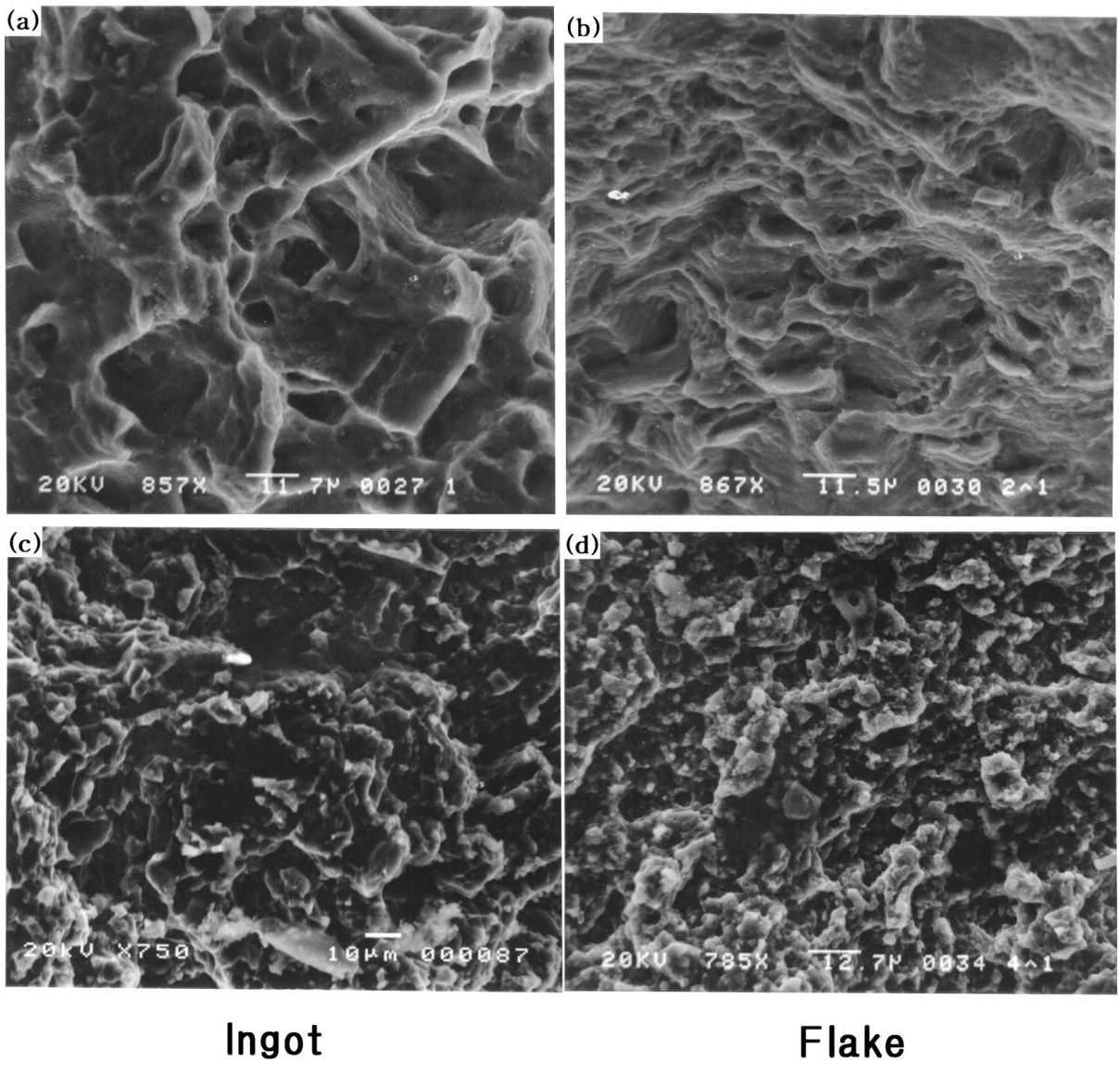

Figure 9 Fracture surfaces of the Mg-5Al and Mg-15Al extrusions from the ingots and flakes. (a) and (b) Mg-5Al, (c) and (d) Mg-15Al.

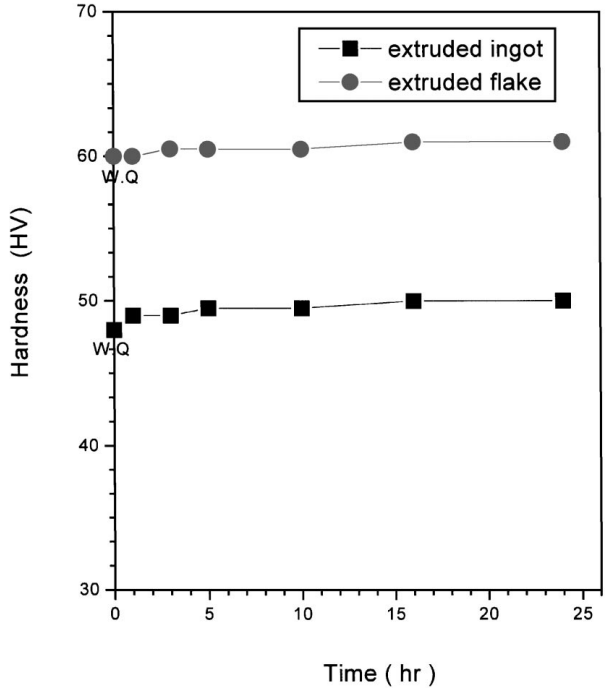

Figure 10 Age hardening behavior of Mg-5Al ingot and flake extrusions at 170 °C. No age hardening is observed.

25%. Further, there is a drastic decrease in elongation from the Mg-5Al to Mg-15Al alloys, both in the ingot and flake extrusions. Ductile fracture was observed in all the alloys and the dimple size is smaller in the RSP material than in the IM material (Fig. 9) and this can be explained on the basis of the finer microstructure of the RSP material.

None of the alloys exhibited any age hardening behavior. The hardness virtually remained constant with time up to at least 24 h at 170 °C (Fig. 10). Since G.P. zones and transition phases do not form in binary Mg-Al alloys, precipitation hardening is not expected to occur in these alloys. An important consequence of the solution treatment at 410 °C and aging at 170 °C is the development of an equiaxed two-phase mixture in all the alloys and the precipitate size is large. A typical pair of micrographs of the Mg-30Al alloy is shown in Fig. 11. It is clear from these micrographs that the microstructure is coarse and therefore any hardening would not have been expected. Solution heat treatment and aging at lower temperatures could have perhaps contributed to some extent of hardening. But, the hardening is mostly due to small grain size and not due to precipitation strengthening.

3.4. Electrochemical behavior

Fig. 12 shows the electrochemical behavior of the Mg-5, 15 and 30 Al alloys in both the ingot and flake extrusions. A comparison between the two sets of curves shows that the flake material has a higher corrosion resistance than the ingot material. This is clear from the decrease in corrosion current by more than an order of magnitude. Similar results have been reported by others [17]. The increased corrosion resistance of RSP Mg-Al alloys has been due to the formation of a magnesium

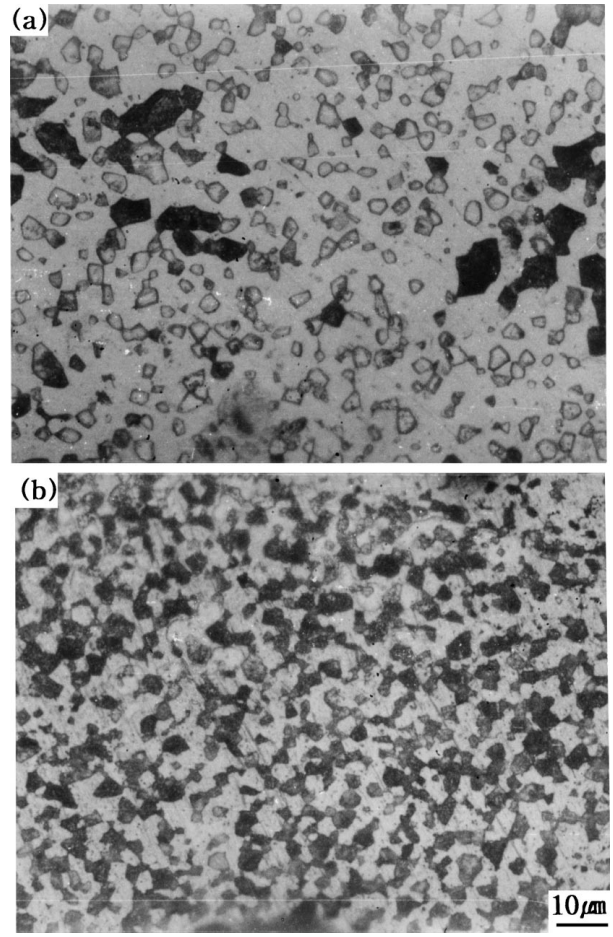

Figure 11 Optical micrographs of the Mg-30Al alloy extrusions solution treated at 410 °C and aged at 170 °C for 16 h. (a) Ingot and (b) flake.

hydroxide on the surface of the samples [18–21]. The increased homogeneity in the RSP condition also is an additional factor in improving the corrosion resistance.

3.5. General comments

From the above results it becomes clear that all the three alloys exhibit finer microstructural features and consequently better mechanical properties in the RSP condition than in the IM condition. However, the extent of improvement in the properties is not very significant. This may be attributed to the following reasons. Firstly, binary Mg-Al alloys do not show any significant age hardening behavior. This is due to the fact that the equilibrium β-$Mg_{17}Al_{12}$ phase precipitates out directly from the supersaturated solid solution. Since G.P. zones and transition phases do not form in this system, no hardening occurs. Secondly, the grain size of the RSP alloys is expected to be significantly smaller than in the conventional cast alloys, usually by a couple of orders of magnitude. But, due to the relatively low rates of solidification during RSP in the present investigation, the undercooling is less and therefore grain refinement is limited. Further, the temperature employed for extrusion is reasonably high and consequently some grain growth could have occurred. The net result is that the final grain size of the extruded material is not that fine. Additionally, the small extent of supersaturation of Al obtained in the RSP alloys is no longer present in the

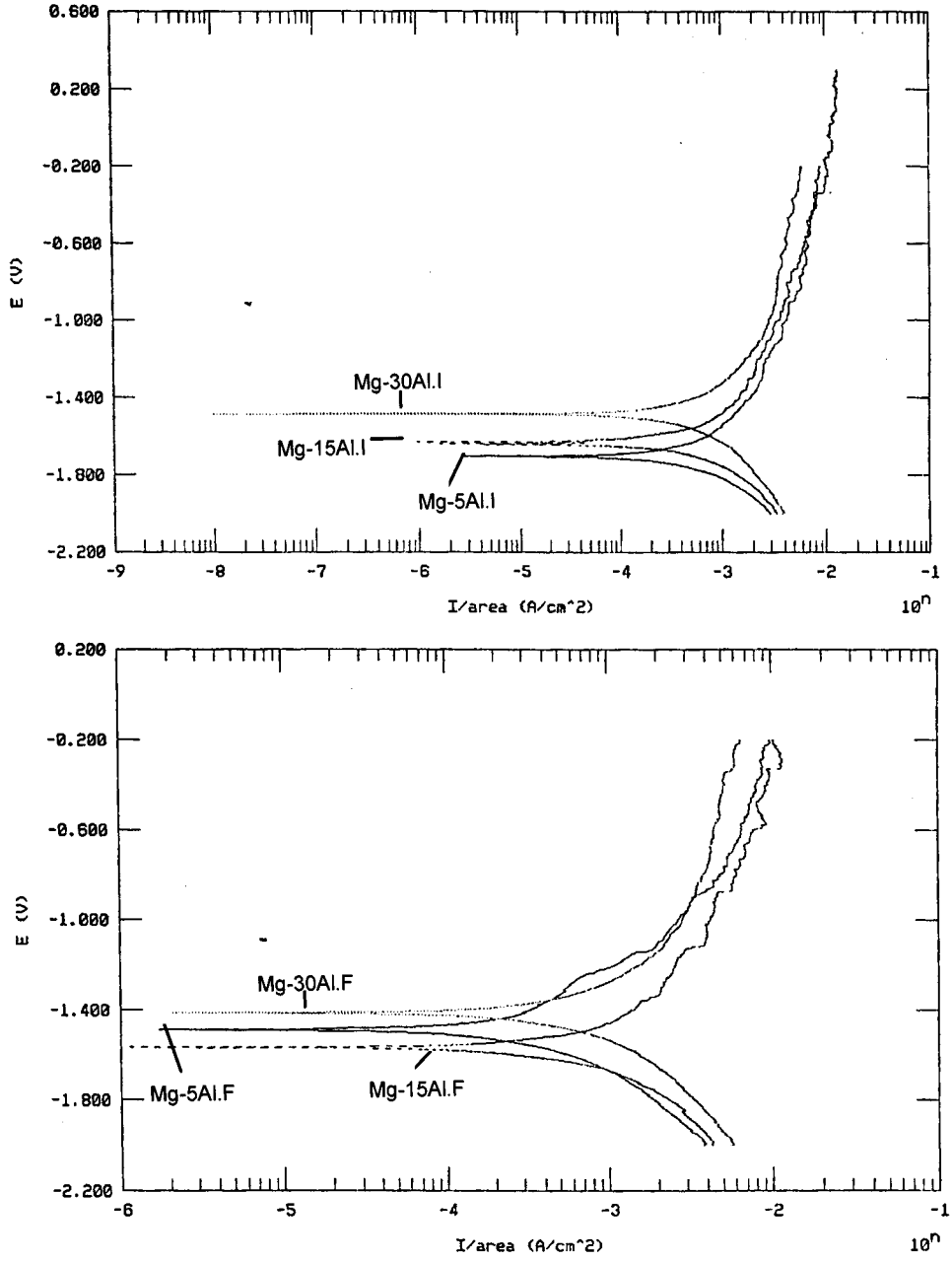

Figure 12 Electrochemical behavior of ingot and flake extrusions of Mg-5, 15, and 30Al alloys. I = ingot, F = flake.

as-extruded condition, again due to the high temperature of extrusion. Thus, the effects of RSP on the mechanical properties are not as pronounced in these alloys as in some other alloys, e.g., those based on aluminum or Mg-Al-Zn alloys containing rare-earth additions.

4. Conclusions

Based on the results presented above for the ingot cast (IM) and rapidly solidified (RSP) binary Mg-Al alloys, the following conclusions can be drawn:

1. The room temperature solid solubility of Al in Mg increased in the RSP binary Mg-Al alloys from the equilibrium value of <1 at % to 10.6 at % Al.

2. The grain size of the α-Mg solid solution phase and the size of the β-$Mg_{17}Al_{12}$ intermetallic were smaller in the RSP alloys than in the IM alloys.

3. Because of the fine size of the α-Mg and β-$Mg_{17}Al_{12}$ phases, the hardness and tensile strength of the RSP alloys were higher than in the IM alloys.

4. No age hardening behavior was observed in the RSP or IM alloys.

5. Since extrusion was carried out at a reasonably high temperature of 290–350 °C, the effects of RSP were partially lost. Consequently, the improvement in hardness and strength was not as high as expected.

References

1. C. SURYANARAYANA (ed.), "Non-equilibrium Processing of Materials" (Elsevier, Oxford, UK, 1999).
2. S. K. DAS, "Reviews in Particulate Materials," Vol. 1 (Metal Powder Industries Federation, Princeton, NJ, 1993) p. 1.
3. H. H. LIEBERMANN (ed.), "Rapidly Solidified Alloys: Processes, Structures, Properties, Applications" (Marcel Dekker, New York, NY, 1993).
4. T. R. ANANTHARAMAN and C. SURYANARAYANA,

"Rapidly Solidified Alloys: A Technological Overview" (Trans Tech Publications, Aedermannsdorf, Switzerland, 1987).
5. C. SURYANARAYANA, F. H. FROES, S. KRISHNAMURTHY and Y. W. KIM, *Int. J. Powder Metallurgy* **26** (1990) 117.
6. T. R. ANANTHARAMAN (ed.), "Metallic Glasses: Structure, Properties, and Applications" (Trans Tech Publications, Aedermannsdorf, Switzerland, 1984).
7. R. W. CAHN, in "Glasses and Amorphous Materials," Materials Science and Technology—A Comprehensive Treatment, Vol. 9, edited by J. Zarzycki (VCH Verlagsgesellschaft GmbH, Weinheim, Germany, 1991) p. 493.
8. L. A. DAVIS, S. K. DAS, J. C. M. LI and M. S. ZEDALIS, *Int. J. Rapid Solidification* **8** (1994) 73.
9. L. A. JACOBSON and J. MCKITTRICK, *Mater. Sci. & Eng. Reports* **R11** (1994) 355.
10. C. SURYANARAYANA, F. H. FROES and R. G. ROWE, *Int. Mater. Rev.* **36** (1991) 85.
11. R. E. LEWIS, A. JOSHI and H. JONES, in "Processing of Structural Metals by Rapid Solidification," edited by F. H. Froes and S. J. Savage (ASM International, Materials Park, OH, 1987) p. 367.
12. C. F. CHANG, S. K. DAS, D. RAYBOULD, R. L. BYE and E. V. LIMONCELLI, *Light Metal Age* **47** (1989) 12.
13. G. NUSSBAUM, P. SAINFORT, G. REGAZZONI and H. GJESTLAND, *Scripta Metall.* **23** (1989) 1079.
14. H. JONES, *Int. J. Rapid Solidification* **4** (1989) 297.
15. I. J. POLMEAR, "Light Alloys," 3rd ed. (Halsted Press, an imprint of John Wiley & Sons, Inc., New York, 1995).
16. J. D. COTTON, *J. Electrochem. Soc.* **136** (1989) 523C.
17. F. HEHMAN, F. SOMMER, H. JONES and R. G. J. EDYVEAN, *J. Mater. Sci.* **24** (1989) 2369.
18. C. B. BALIGA, P. TSAKIROPOULOS and C. JEYNES, *ibid.* **26** (1991) 1497.
19. C. B. BALIGA and P. TSAKIROPOULOS, *Mater. Sci. & Eng.* **A134** (1991) 1029.
20. G. L. MAKAR, J. KRUGER and K. SIERADZKI, *J. Electrochem. Soc.* **139** (1992) 47.
21. *Idem., Corrosion Sci.* **34** (1993) 1311.
22. T. B. MASSALSKI, H. OKAMOTO, P. R. SUBRAMANIAN and L. KACPRZAK, "Binary Phase Diagrams," Vol. 1, 2nd ed. (ASM International, Materials Park, OH, 1990) p. 170.
23. H. L. LUO, C. C. CHAO and P. DUWEZ, *Trans. TMS-AIME* **230** (1964) 1488.
24. C. SURYANARAYANA, in "Processing of Metals and Alloys," Materials Science and Technology—A Comprehensive Treatment, Vol. 15, edited by R. W. Cahn (VCH Verlagsgesellschaft GmbH, Weinheim, Germany, 1991), p. 57.
25. H. JONES, "Rapid Solidification of Metals and Alloys" (Institution of Metallurgists, London, UK, 1982).
26. E. LAINE and I. LÄHTEENMÄKI, *J. Mater. Sci.* **6** (1971) 1418.
27. T. Z. KATTAMIS, U. T. HOLMBERG and M. C. FLEMINGS, *J. Inst. Metals* **95** (1967) 343.

Received 20 August 1997
and accepted 24 February 1999